Eur. Phys. J. B **28**, 341–352 (2002)
DOI: 10.1140/epjb/e2002-00237-3

THE EUROPEAN PHYSICAL JOURNAL B

Selection of dune shapes and velocities Part 2: A two-dimensional modelling

B. Andreotti[1,a], P. Claudin[2], and S. Douady[1]

[1] Laboratoire de Physique Statistique de l'École Normale Supérieure, 24 rue Lhomond, 75231 Paris Cedex 05, France
[2] Laboratoire des Milieux Désordonnés et Hétérogènes[b], 4 place Jussieu - case 86, 75252 Paris Cedex 05, France

Received 22 December 2001 / Received in final form 31 May 2002
Published online 31 July 2002 –

Abstract. We present in this paper a simplification of the dune model proposed by Sauermann *et al.* which keeps the basic mechanisms but allows analytical and parametric studies. Two kinds of purely propagative two dimensional solutions are exhibited: dunes and domes. The latter, by contrast to the former, do not present a slip face. Their shape and velocity can be predicted as a function of their size. We recover that dune profiles are not scale invariant (small dunes are flatter than the large ones), and that the inverse of the velocity grows almost linearly with the dune size. We furthermore get the existence of a critical mass below which no dune solution exists. It rises the problem of dune nucleation: how can dunes appear if any bump below this minimal mass gets eroded and disappears? The linear stability analysis of a flat sand bed shows that it is unstable at large wavelengths: dune can in fact nucleate from a small sand mass if the proto-dune is sufficiently long.

PACS. 45.70.-n Granular systems – 47.54.+r Pattern selection; pattern formation

1 Introduction

The beauty of the crescentic barchan dunes have recently attracted the interest of physicists for a better understanding and modelling of sand transport, as well as ripples and dunes formation and propagation. E. Guyon had this witty remark: 'barchans are our drosophila', meaning that beyond the scientific and fundamental works on these dunes, we all keep in mind that such studies may lead to potential applications in the fight of saharan countries against sand invasion. One of the first reference work in the field is certainly the famous book of Bagnold which dates back from 1941 [1]. Since then, a great effort of measurement and modelling has been done which we have reviewed in details in the first part of these twin papers.

Our aim here is to discuss and model the selection of two-dimensional dune shape and velocity. For that purpose, we will simplify the model proposed by Sauermann *et al.* [2–5]. We will show that although making rather severe approximations, we are able to recover their main results, in particular that dune profiles are not scale invariant, and that the inverse of the velocity grows almost linearly with the dune size. Besides, analytical expressions of dome and dune profiles can be obtained, but whose coefficients have to be numerically computed.

We furthermore get the existence of a critical size below which no dune solution exists. This minimal size directly rises the problem of dune nucleation: how can a dune appear if any bump below a critical mass is eroded and disappears? We give here the linear stability analysis of a flat sand bed and show that it is unconditionally unstable towards large wavelengths perturbations. This means that a dune can nucleate from a very small sand mass, if sufficiently long.

The paper is organized as follows. Section 2 is devoted to the equations of the model. The linear stability of a uniform sand sheet is treated in Section 3. In Section 4.1 we simplify further the equations and show what is the general shape of the purely propagative solutions of the model. The specific case of domes and 'actual' dunes are discussed in Sections 4.2 and 4.3 respectively. At last, we conclude with a discussion of the relevance of these results, and the possible extension of the model to three-dimensional situations and to dynamical studies.

2 Basic equations

2.1 Continuity and charge equations

We wish to give a description of the shape and evolution of two-dimensional dunes in terms of two fields: the profile $h(x,t)$ and the volumic sand flux $q(x,t)$ which is the volume of sand transported through an infinite vertical line

[a] e-mail: andreott@lps.ens.fr
[b] (UMR 7603)

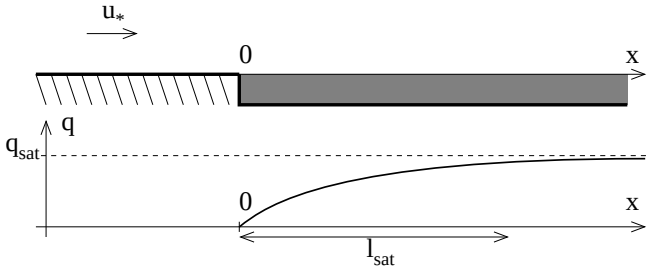

Fig. 1. The wind cannot transport more than a given sand flux, called the saturated flux, which depends only on the wind strength. When the wind is blowing on a patch of sand, the flux gets saturated after a typical length l_{sat}. This saturation length l_{sat}, which turns out to be almost independent of the wind shear velocity u_* – see Part 1 – is the only relevant lengthscale in the problem.

per unit time. x denotes the horizontal coordinate and t is the time. We are going to write a set of three equations for these quantities in order to include into the model (i) the mass conservation, (ii) the progressive saturation of sand transport and (iii) the feedback of the topography on the sand erosion/deposition processes. Although we shall restrict ourselves in this paper to two-dimensional situations corresponding to transverse dunes (invariant in the direction perpendicular to the wind), our ultimate goal is of course to be able to describe three dimensional dunes and barchans in particular.

Because barchans migrating in dune fields organize themselves like gooses or ducks during their migration flights, we named this class of models the $\mathsf{C}^{\mathsf{C}}_{\mathsf{C}}$ modelling. This denomination includes the approach of Sauermann *et al.* as well as the different variations and simplifications we derive in this paper from their work. At this stage of the modelling, we are however far from being able to take into account such 'interactions' between dunes which are necessary to explain the $\mathsf{C}^{\mathsf{C}}_{\mathsf{C}}$ spatial organisation, and we shall focus on isolated objects only.

A simple balance calculation shows that the erosion rate $-\partial_t h$ is directly related to the divergence of the flux q. This gives the common continuity equation:

$$\partial_t h + \partial_x q = 0. \tag{1}$$

The saturation effect of the sand transport has been already discussed in the first part of these twin papers. Consider a patch of sand on which the wind is blowing – see Figure 1. The flux of transported sand q first increases and, because of the feedback of the grains on the wind velocity profile, get saturated after a typical length l_{sat}. In the first part of the paper, we showed that $l_{sat} = \xi d\, \rho_{sand}/\rho_{air}$ (d is the grain diameter, ρ the densities and ξ a non dimensional prefactor), *i.e.* is almost independent of the wind shear velocity u_* – slow logarithmic dependencies hidden in ξ only. This phenomenon has been reported and studied by several authors, *e.g.* [1,6]. The real shape of $q(x)$ is certainly more complicated than the one drawn in Figure 1. In particular, oscillating or overshooting features were reported in [1] when q reaches its asymptote. However, what is important for our purpose is only that a saturated value q_{sat} is reached after a length l_{sat}. This space lag is satisfactorily described by the following equation:

$$\partial_x q = \frac{q_{sat} - q}{l_{sat}}\,. \tag{2}$$

This charge equation can be seen as a simplification of that proposed by Sauermann *et al.* in their continuum saltation model [3]. An important remark is that this equation is valid only if *some grains are available on the sand bed*. On a firm soil indeed, the flux cannot increase to become saturated. As suggested by Peer and Hakim [7], the right hand side of equation (2) must be therefore multiplied by some matching function which quickly tends to zero when the altitude h above the firm soil is decreased below, say, d the grain diameter, and which is equal to unity above this value. Then, the equation (2) becomes non linear but no boundary conditions have to be specified at the edges of the sand covered region. For example, if the matching function tends to zero like h, the dune will always keep a thin sand sheet at its back. But if it varies as $\sqrt{h}$, the dune will have a finite extension and will join the firm soil with an horizontal tangent. We shall ignore at present these subtleties but keep them in mind to invoke them later when necessary.

Another important remark is that the time scale on which the dune profile h evolves is incomparably larger than that of the sand flux q. We then assume that q adapts its profile instantaneously according to equation (2) and makes h change slowly through equation (1). Therefore any term $\partial_t q$ is irrelevant in this modelling.

2.2 Relationship between dune shape and sand flux

The saturated flux q_{sat} is uniform for a flat sand bed only. To the first order, the saturated flux q_{sat} is a function of the local shear stress $\tau = \rho_{air} u_*^2$ which itself depends – non locally – on the topography: basically, bumps and upwind slopes get more eroded than dips and downwind faces. A classical relationship between the saturated flux q_{sat} and the shear velocity u_* that can be recovered with the scaling arguments of the Part 1 of the paper is:

$$q_{sat} \propto \frac{\rho_{air}}{\rho_{sand}} \frac{u_*^3}{g}\,. \tag{3}$$

In principle, such a relationship is valid far from the velocity threshold u_{thr} under which no sand can be transported by the wind, *i.e.* $q_{sat} = 0$ for $u_* \leq u_{thr}$. Refined formulas can be obtained which essentially smooth the step from 0 to the previous asymptotic expression such as that obtained in Part 1:

$$q_{sat} \propto \frac{\rho_{air}}{\rho_{sand}} \frac{u_*}{g} \left(u_*^2 - u_{thr}^2\right). \tag{4}$$

In the whole range $-u_{thr} < u_* < u_{thr}$, q_{sat} is null so that in practice, q_{sat} cannot become negative on a dune. This condition will be used in Section 4.2.

To close the equations, we have to explicit the spatial variations of the turbulent wind velocity due to the dune profile. The simplest model which verifies the basic requirements (see Part 1) is certainly the perturbative calculation by Jackson and Hunt [8,9]. Neglecting logarithmic scale dependencies, Kroy *et al.* [4,5] have extracted the main features of their work by expressing the shear velocity as:

$$\frac{u_*^2(x)}{U_*^2} = 1 + A \int \frac{\mathrm{d}\chi}{\pi\chi}\, \partial_x h(x-\chi) + B\, \partial_x h(x), \qquad (5)$$

where U_* is the shear velocity exerted on a flat bed. First, it must be noted that the convolution integral acts on $\partial_x h$ roughly like a derivative, leading to a term which encodes curvature effects. But this curvature is dimensionless and thus does not depend on the dune size – in other words, this term can be seen as a curvature rescaled by the dune size. It reflects the observation that the wind velocity increases on bumps (negative curvature) and decreases on hollows (positive curvature). Second, it is a non local term, meaning that the shear velocity depends on the whole shape of the dune. Of course sharp variations of the dune profile will also have a strong local effect. At last, the second (B) term simply takes into account slope effects: positive slopes are more eroded than negative ones. Again, this term does not introduce any new lengthscale.

Expression (5) can be used to close up the set of equations as was done by Kroy *et al.* in [4,5] who used besides a more sophisticated – and non-linear – charge equation than (2). It is useful to simplify further the equation linking q_{sat} to h without loosing too much physics, in order to let more analytical developments. The linear expansion of the expression (5) rewritten in terms of $q_{sat} \propto u_*^3$ gives:

$$\frac{q_{sat}(x)}{Q_{sat}} = 1 + \frac{3}{2} A \int \frac{\mathrm{d}\chi}{\pi\chi}\, \partial_x h(x-\chi) + \frac{3}{2} B\, \partial_x h(x), \qquad (6)$$

and is fully justified by the approximations under which equation (5) is valid. By definition, $Q_{sat} = q_{sat}(U_*)$ is the saturated flux on a flat sand bed submitted to a shear velocity U_*.

As discussed in Part 1, A and B are not strictly constant but increase with the logarithm of the ratio of the dune size D to the roughness of the sand surface z_0. For D varying between 20 m and 200 m and a roughness of order of the grain size, $\ln(D/z_0)$ does not change by more than 20%. A reasonable approximation is thus to take constant values for the coefficients A and B. Moreover, the aspect ratio of actual dunes (around 0.1 for the height to length ratio) is too large to justify completely the approximations [4,5,8,9] necessary to derive expression (6). We nonetheless think that it is sufficient in the present state, provided that A and B become effective parameters. In the following, we will use $A = 6$ and $B = 4$ which are, in view of the results, reasonable values of the parameters A and B.

Furthermore, we shall use the saturation length l_{sat} and flux Q_{sat} to make our variables dimensionless. Thus, for a given wind shear velocity, all relevant scales of the problem are fixed. For instance, Q_{sat}/l_{sat} is the velocity scale, l_{sat}^2/Q_{sat} the time scale, Q_{sat}/l_{sat}^2 the frequency scale, etc. Note that the strength of the wind is completely absorbed in these rescalings.

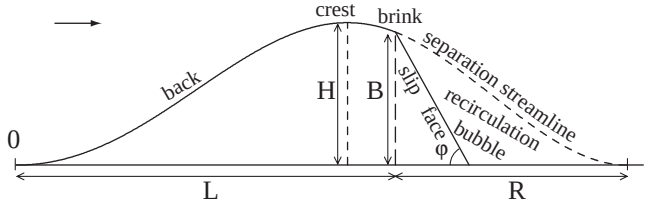

Fig. 2. The sand transport increases on the back of the dune which is thus eroded. The sand is deposed at the brink and is redistributed along the slip face by avalanches. It can be assumed that the slip face is always at the repose angle φ. At the brink, the turbulent boundary layer separates from the dune, enclosing a recirculation bubble. In the absence of better approximations, the separation streamline is assumed to extend the dune profile and to reattach the ground smoothly. By definition, L is the distance between the foot of the dune ($x = 0$) and the brink $x = L$, H is the height of the highest point of the dune (crest) and B is the dune height at the brink. H and B may coincide or not.

2.3 The recirculation bubble

It is a common field observation (see Part 1) that the wind streamlines on a dune follow exactly the shape of its back profile but separate at the point where the avalanche slip face begins – the brink – and reattach further downwind, see Figure 2. This phenomenon creates an eddy recirculation in the 'shadow' of the dune, where the wind is much less strong than anywhere else. As a consequence, all the sand eroded on the back is deposited around the top of the slip face which avalanches when the slope becomes too steep. As explained in the first part of these twin papers, it is fortunate that an accurate description of these avalanches is not necessary due to the fact that they do not have any feedback on the back profile of the dune: they simply relax the slope to its equilibrium value $\tan\varphi$. We will use the value $\varphi = 30°$ in the following, as usually measured for desert sand.

The simplest way to model the feedback of the recirculation bubble on the whole dune has been proposed by Zeman and Jensen [12] and used more recently by Kroy *et al.* [4,5]. The idea is to build an envelope of the dune which prolongs the dune profile by the separation streamline – see Figure 2. To the first order, the wind on the back of the dune is the same as that would have been obtained if the envelope was solid. For example, the convolution integral in equation (5) used to calculate the shear stress on the soil should be applied not to the dune profile only, but to the dune + bubble envelope.

Following Kroy *et al.* [4,5], we are going to build a very simple – yet empirical – separation streamline $h_b(x)$, written as a polynomial of 3rd degree. The conditions under which the turbulent boundary layer separates from the dune cannot be easily expressed and even are not clear at

all. It is a common observation that the flow separation occurs on the downwind face of a bump if the downslope is sufficiently large. Thus, the simplest empirical criterion is that the slope be locally steeper than some threshold value $-\mu_b$. In the sequel, we shall use the typical value $\mu_b = 0.25$.

Another basic requirement is that the junction at the brink ($x = L$) and at the reattachment point with the soil ($x = L + R$) be smooth (see Fig. 2). This already gives four relationships: $h_b(L) = h(L) \equiv B$, $h_b'(L) = h'(L) \equiv p$, $h_b(L + R) = h(L + R)$ and $h_b'(L + R) = h'(L + R)$. To be self consistent, the separation streamline should be nowhere steeper than the critical slope $-\mu_b$. As a consequence, the recirculation bubble nucleates at null size, the first time the dune slope becomes steeper than $-\mu_b$. It is natural to impose that the steepest slope along the separation streamline – at the inflexion point x_b, defined by $h_b''(x_b) = 0$ – be strictly equal to $-\mu_b$:

$$h_b'(x_b) = -\mu_b. \tag{7}$$

This last condition selects the length R of the recirculation bubble.

In most of the cases, the boundary layer reattaches on the flat soil downwind the dune ($h(L + R) = 0$ and $h'(L + R) = 0$) and the separation streamline becomes:

$$h_b(x) = \left(1 - \frac{x - L}{R}\right)^2 \left(B + (pR + 2B)\frac{x - L}{R}\right) \cdot \tag{8}$$

Using the condition (7), the length R of the recirculation bubble can be expressed as:

$$\frac{R}{3B} = \frac{\mu_b - p - \sqrt{\mu_b(\mu_b + p)}}{p(p - 3\mu_b)} \tag{9}$$

R scales on the height B at the brink but depends on the slope p: as expected, the recirculation bubble is scale invariant but of course depends on the shape of the dune.

3 Stability of a flat sand bed

Before going further in the modelling of dune shape and propagation, we wish to investigate the problem of dune initiation. Indeed, as reported in the first part, there are two striking field observations. First, no persistent barchan dunes exist smaller than say, 1 m high, 20 m large and 20 m long. Second, any small conical sandpile blown by the wind disappears even when a sand supply is provided. Then, how can barchan dunes appear?

To investigate this problem, we have integrated numerically equations (1, 2, 6) for two initial conditions. First, a small triangular sandpile at the repose angle is prepared on the firm soil (Fig. 3). It can be seen that it is rapidly eroded and disappears, as observed in the field and in wind tunnel experiments – see Part 1. Second, we look at the evolution of a thin sand sheet (Fig. 4) disturbed by a flat bump. This initial condition mimics a sand beach on which sand is deposed by water. It can be seen that the bump

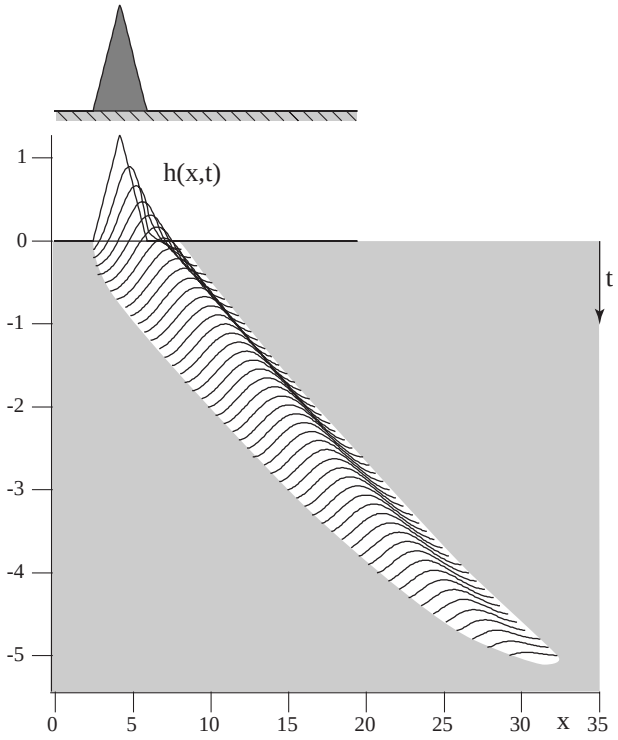

Fig. 3. Time evolution of a small triangular sandpile on the firm soil, initially 1.3 l_{sat} high and at the repose angle. The pile is quickly eroded and after some time, all the amount of sand available at $t = 0$ (grey filled region) is swept out. The field observation that such a small sandpile disappears is thus recovered in the model. The graph results from the numerical integration of equations (1, 2, 6) with $A = 6$ and $B = 4$. $h(x, t)$ and x are in units of l_{sat}. The time between two profiles is 0.1 in units of l_{sat}^2/Q_{sat}. For legibility, the profiles are translated vertically from time to time.

propagates downwind and induces a strong erosion of the sand bed in front of it. A second bump nucleates from the initial perturbation which itself induces a strong erosion in front of it, and so on. After some time, a series of growing oscillations is generated. The amplification of this phenomenon stops when the oscillations eventually reach the firm soil from which no sand can be eroded, and/or when recirculation bubbles appear. As a conclusion, depending on their spatial extension, small sand bumps either disappear or grow and initiate dunes.

It is then instructive to make the linear stability analysis of a flat sand bed. Let us consider an infinite uniform sand bed blown by a uniform wind. The sand flux is everywhere saturated: $q = 1$ (in units of Q_{sat}). To investigate its stability, we can consider, without loss of generality a small perturbation of the form:

$$h(x, t) = H\mathrm{e}^{\sigma t - \mathrm{i}\omega t + \mathrm{i}kx}, \tag{10}$$

$$q(x, t) = 1 + Q\mathrm{e}^{\sigma t - \mathrm{i}\omega t + \mathrm{i}kx}, \tag{11}$$

where Q and H are related one to the other by the conservation of matter, $(\mathrm{i}\omega - \sigma)H = \mathrm{i}kQ$. From the relation (6), we get the following expression for the saturated

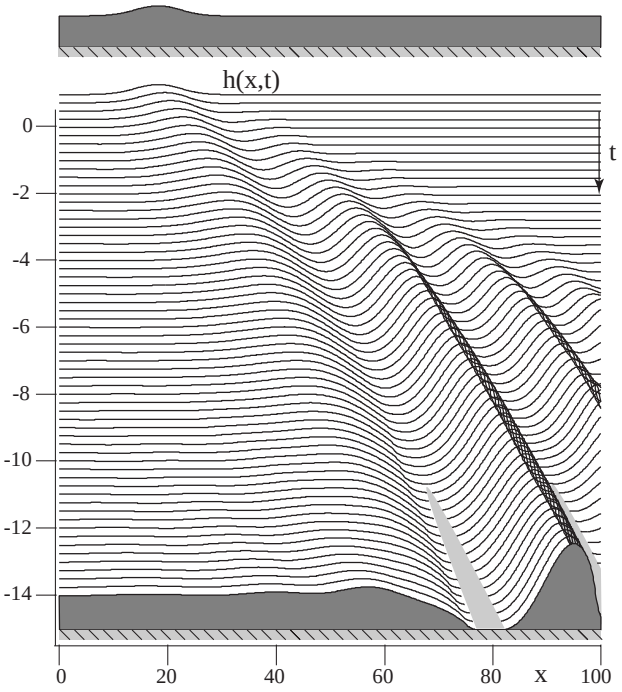

Fig. 4. Time evolution of a flat sand sheet of height l_{sat} above the firm soil disturbed by a small hump. The perturbation propagates downwind and induces the growth of oscillations downwind it. The hollow created in front of the initial bump soon reaches the firm soil: the initial sand bed (grey filled region) divides into an array of isolated dunes. Except the time between two profiles which is 0.5, the details are the same than for Figure 3.

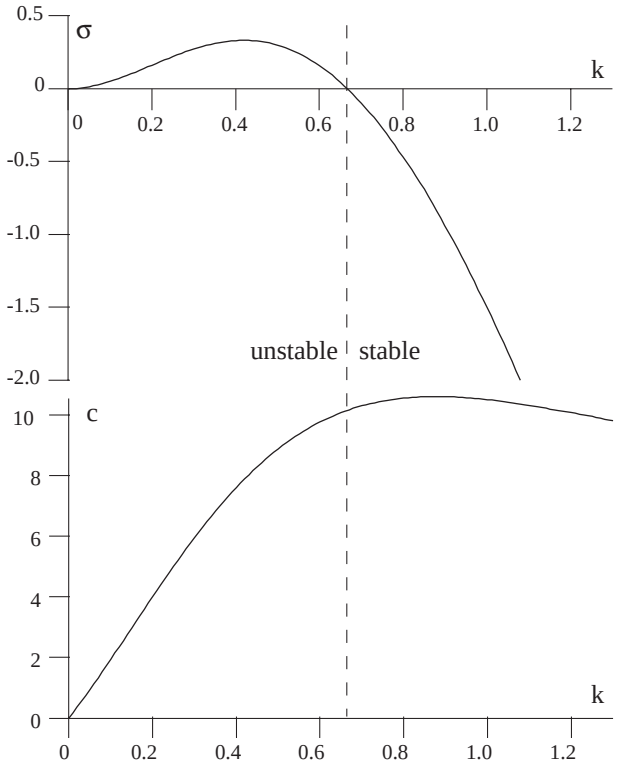

Fig. 5. Results of the linear stability of a uniform sand bed blown by the wind, for $A = 6$ and $B = 4$. Top: growth rate σ, rescaled by Q_{sat}/l_{sat}^2, as a function of the disturbance wave number k, rescaled by $1/l_{sat}$. The sand bed exhibits a large wavelength instability. Bottom: group velocity c of disturbances, rescaled by Q_{sat}/l_{sat}, as a function of the disturbance wave number k, rescaled again by $1/l_{sat}$. For small wave numbers, the velocity c increases linearly with k and thus decreases as the inverse of the wavelength.

flux: $q_{sat} = 1+3/2(A|k|+Bik)h$. Once replaced in the saturation equation, it gives: $(1+\mathrm{i}k)Q = 3/2\ (A|k|+Bik)H$. Combining these equations we finally obtain:

$$\sigma = \frac{3k^2(B - A|k|)}{2(1+k^2)}, \tag{12}$$

$$\omega = \frac{3k|k|(A + B|k|)}{2(1+k^2)}. \tag{13}$$

Note that a more complicated relation between q_{sat} and u_* than (3) would only affect the prefactor, *i.e.* the time scale, in this calculation.

As shown in Figure 5 (top), the growth rate σ is positive for small wavenumbers ($k < B/A$) and negative for large wavenumbers ($k > B/A$). A flat sand bed thus exhibits a large wavelength instability which can explain the initiation of dunes. But it is stable towards small wavelength disturbances, so that a small sandpile on a firm soil is quickly eroded.

For wavelengths much larger than the saturation length the previous equations simplify in $\omega \simeq 3/2\ Ak^2$ and $\sigma \simeq 3/2\ Bk^2$. The A and B terms in equations (5) and (6) thus corresponds to the mechanisms responsible respectively for the propagation and for the growth of disturbance. Consider a symmetric bump (like a bell curve). Due to the curvature dependence of the wind (A term), the flux increases on the upwind face of the hump and decreases on the downwind face. The upwind face is thus eroded and the sand is deposed progressively on the downwind face. As a consequence, the curvature dependence of the wind is responsible for the propagation of the hump. Now, due to the dependence of the wind on the slope (B term), the flux is slightly larger upwind the bump maximum than downwind. In the frame of reference of the bump, there is thus a net flux towards the maximum of the bump: the hump grows. Finally the lag before saturation introduces a cut-off for lengthscales smaller than the saturation length: a bump shorter than l_{sat} gets eroded since the flux is not saturated.

The fastest growing mode – that which maximises σ – is obtained for $3k + k^3 = 2B/A$. Neglecting the k^3 term, we obtain a still good approximation of the most unstable wavelength: $\lambda = 2\pi/k \simeq 3\pi l_{sat}A/B$. λ is thus of the order of ten times the saturation length. For $A = 6$, $B = 4$ and $l_{sat} \simeq 9$ m we get a wavelength of 125 m which is reasonable compared to what is observed on transverse dune fields in deserts. Under water l_{sat} rather scales on the grain size and we have $l_{sat} \simeq 1$ cm which gives 14 cm,

again a good estimation of what has been measured by Betat *et al.* [10] or Andersen *et al.* [11] for example.

Finally, it can be seen from equation (13) that disturbances propagate downwind. We can compute the group velocity of these surface waves:

$$c = \frac{\mathrm{d}\omega}{\mathrm{d}k} = \frac{3[A|k| + Bk^2(3+k^2)]}{2(1+k^2)^2}\,. \qquad (14)$$

For small wavenumbers k, the group velocity c increases linearly with k (Fig. 5 (bottom)). This means that for asymptotically large wavelengths λ, the propagation speed scales as Q_{sat}/λ. We thus recover in the limit of large bumps, the scaling proposed by Bagnold for dunes. We also see that the velocity deviates significantly from this law, when the wavelength becomes comparable to the saturation length l_{sat}. This is also the case for actual dunes – see Part 1.

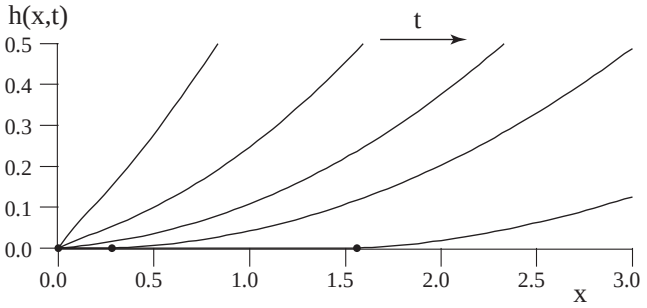

Fig. 6. Time evolution of the foot of the dune (upwind) for an initial sand pile making a finite angle with the firm soil. The profile first flattens and the propagation of the upwind edge only starts when the slope is horizontal. So, equations (6, 15, 16) select dynamically a smooth join between the soil and the dune. The displayed profiles corresponds from left to right to the times $t = 0$, 0.25, 0.5, 0.75 and 1.5.

4 Dunes as solitary waves

4.1 A simple 2d modelling

The expression (6) can be easily used only if the analysis in Fourier space is possible (like for the linear stability analysis). But we wish now to compute the shape and velocity of purely propagative dunes which are localised in space. For simplicity, we will thus replace the convolution expression by a simpler anzats. Since it is a 'scaleless and non-local curvature', we can formally replace it by $-D\partial_{xx}h$, where D is the dune length. We then end up with the following set of linear equations:

$$\partial_t h + \partial_x q = 0, \qquad (15)$$

$$\partial_x q = q_{sat} - q, \qquad (16)$$

$$q_{sat} = 1 - \alpha D\partial_{xx}h + \beta\partial_x h. \qquad (17)$$

Again, α and β should be thought of as phenomenological parameters of order unity reflecting the dependence of the flux on the curvature and the slope respectively. Let us recall that they respectively induce the propagation of a bump (α term) and its growth (β term). Due to the lag before saturation of the sand transport, the α term has also a stabilizing role at small lengthscales. The rescalings $h \leftarrow \alpha h$ and $t \leftarrow \alpha t$ (with q and x unchanged) shows that only the ratio β/α is actually important. At last, as we already mentioned, the charge equation (16) is valid only if there is some sand to be eroded $h > 0$. Note also that the expression (17) of the saturated flux is valid only if it is positive: q_{sat} should be taken as null if the expression is negative.

The boundary conditions are implicitly determined when the expression (6) of q_{sat} – that which involves the convolution – is used. Indeed, the wind velocity field and thus the saturated flux do not feel the difference between the firm soil and the dune. The 'free' surface profile should thus be considered as a whole. Figure 6 shows the evolution of the upwind edge of a dune. The profile quickly becomes flat and only then, the dune starts propagating. The same argument is valid for the simplified equation (17). If the slope h' was not continuous at the dune edge, in some sense, h'' would be infinite. Then, from equation (17), the saturated flux would formally tend to $-\infty$ over a region around this edge, *i.e.* would be forced to be null because it cannot be negative. Thus in this region, only sand deposition is permitted. This means that a discontinuity in the slope at the dune edge, immediately reacts to prevent the motion of this boundary point, which starts moving again only when the profile becomes flat. There is thus a dynamical selection of the boundary condition: the profile h as well as its slope h' should vanish at the upwind boundary of the dune.

In the following, we are going to look for solitary waves *i.e.* functions of the type $h(x-ct)$ and $q(x-ct)$. We now describe everything in the frame of reference of the dune and rename x as the new space coordinate. Under this steady state hypothesis, the continuity equation (15) can be easily integrated and gives:

$$q = q_0 + ch. \qquad (18)$$

q_0 is the sand supply *i.e.* the incoming sand flux at the point $x = 0$ at which the dune starts ($h = 0$). Upwind the dune ($x < 0$), no grains are available on the ground: $h = 0$ and $q = q_0$ everywhere. For the dune itself ($x > 0$), we use the relation (18) between q and h in the charge equation (16) together with q_{sat} given by expression (17) and we get an ordinary differential equation for the dune profile $h(x)$:

$$1 - \alpha D h'' + (\beta - c)h' - ch - q_0 = 0, \qquad (19)$$

where h' and h'' denote the first and second derivatives of the dune profile. Under the two boundary conditions $h(0) = 0$ and $h'(0) = 0$, the solution of equation (19) is

$$h(x) = \frac{1-q_0}{c}\left[1 + \left(\frac{s}{k}\sin(kx) - \cos(kx)\right)\mathrm{e}^{sx}\right], \qquad (20)$$

where the coefficients s and k are given by

$$s = \frac{\beta - c}{2\alpha D}, \qquad k = \frac{1}{2\alpha D}\sqrt{4c\alpha D - (\beta - c)^2}. \qquad (21)$$

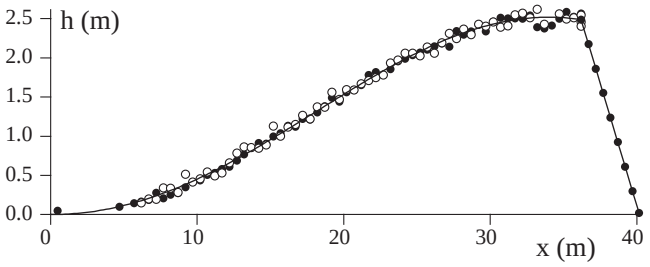

Fig. 7. Longitudinal profile of a barchan dune at Negrita beach, southern Morocco. Black and white dots correspond to independent measurements of the same dune. The solid line correspond to the best fit by a function of the form (20).

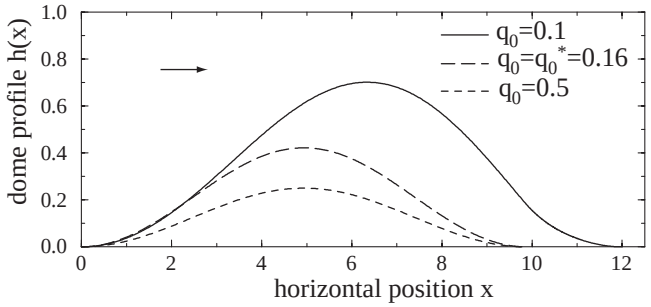

Fig. 8. Shape of the dome solution for different values of the sand flux q_0, for $\alpha = 1$ and $\beta = 4$. Note the asymmetry upwind/downwind of the low flux dome. For clarity the scale of the vertical axis is much larger than that of the horizontal one.

Having used the upwind boundary conditions only, the solutions are still parametrized by the dune length D and its velocity c which must be fixed by the downwind conditions. Two kinds of right boundary conditions will be considered, leading to so-called 'dome dunes', *i.e.* without avalanche slip face, or 'actual' ones for which the 'recirculation bubble' will be introduced.

Figure 7 shows the comparison between the central longitudinal profile of an actual barchan and the theoretical form (20) which is parametrised by k, s and c. It can be seen that the shape of the dune as well as the upwind boundary conditions are well captured by the model.

4.2 Domes

In this section, we look for domes, which by definition do not show any slip face. Let us first exhibit a particular solution. For the value of the propagation speed $c = \beta$, s vanishes so that the solution (20) reduces to

$$h(x) = \frac{1 - q_0}{\beta} \left(1 - \cos(kx)\right) \tag{22}$$

with $k = \sqrt{\beta/\alpha D}$. The height $h(x)$ vanishes at the position $x = 2\pi/k$ so that the length D of the dome is selected as $D = 4\pi^2\alpha/\beta$. Since the 'natural' downwind boundary conditions $h'(D) = 0$ is verified, it is a solution whatever the sand supply q_0.

In fact, two further conditions should be fulfilled. First, to insure the self-consistency of the solution, the local slope of the dome should be nowhere steeper than $-\mu_b$, value above which, as assumed above, the turbulent boundary layer separates from the dune profile, leading to a slip face. The steepest slope of the dome solution (22) is given by $(q_0 - 1)/2\pi\alpha$, so that q_0 must be larger than $1 - 2\pi\alpha\mu_b$. Second, the expression (17) of the saturated flux q_{sat} is valid only when it remains positive everywhere. As a matter of fact, there is a minimum value of q_0 below which q_{sat} takes negative values and makes this solution inconsistent. It is easy to show that this lower bound for q_0 reads $q_0^* = 1 - \left(1 + (\beta/2\pi\alpha)^2\right)^{-1/2}$. With the values of the parameters α, β and μ_b that we chose, the last of these two conditions is the more restrictive for the solution (22).

For a sand supply q_0 smaller than q_0^*, the dome solution is slightly more complicated and has a velocity $c < \beta$. It presents a small region where the saturated flux is null which corresponds physically to a zone where the wind is below the threshold of motion of the grains. The detailed derivation of this low flux dome solution is given in appendix. Our purpose is rather to give here their main properties, only. The shape difference between high and low flux domes is shown in Figure 8.

For each sand supply q_0, the mass of the corresponding dome can be computed as:

$$M = \int_0^D \mathrm{d}x\, h(x). \tag{23}$$

For $q_0 > q_0^*$ – and $c = \beta$ – this mass can be simply expressed as $M = 4\pi^2\alpha(1 - q_0)/\beta^2$. For $q_0 < q_0^*$ it has to be computed numerically (see Appendix). The resulting curve $M(q_0)$ is shown in Figure 9. The most important point is that the mass is a decreasing function of the flux. Consider a dome propagating in its steady state under a flux q_0. Suppose that its mass slightly increases. The flux of sand which leaves the dome gets smaller than q_0. As a consequence, the dome grows. In the same way, if the mass slightly decreases, the output flux gets larger than q_0 so that the mass further decreases. The dome solution is thus an unstable steady state: domes may either quickly disappear or reach the point where their slope is steep enough to generate a recirculation bubble and create an avalanche slip face to become an actual dune. Note however that the domes may be stabilised either by the interaction with other structures or by the use of periodic boundary conditions, for which the output and input fluxes are coupled [10].

Among the interesting properties of domes, their propagation speed c, shown in the inset of Figure 9, is independent of the dune size for $q_0 > q_0^*$ (small masses) but decreases with it for $q_0 < q_0^*$ (large domes). More precisely, we find in this last case that the inverse of the velocity $1/c$ grows almost linearly with the size $M^{1/2}$ (or the length D).

We have shown in the Section 3 that a too small sandpile is inexorably eroded by the wind. The domes, which are unstable steady solutions, can thus be interpreted in the context of dunes nucleation: for a given flux q_0 the

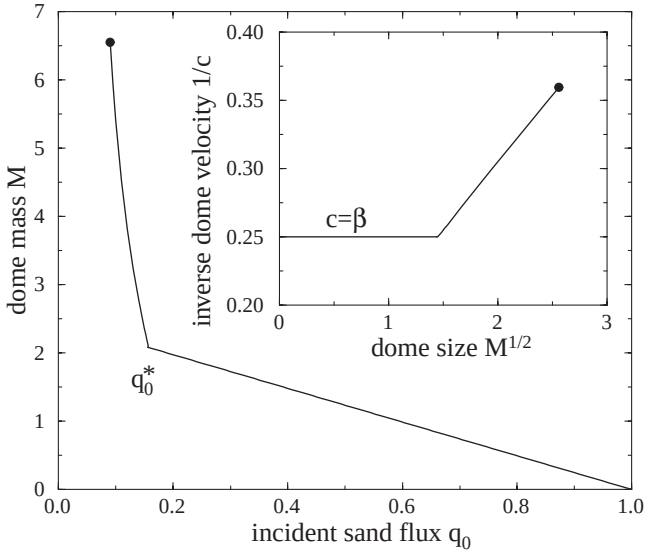

Fig. 9. The main graph shows the mass of a dome selected by an incident flux q_0. This function is a straight line for $q_0 \geq q_0^*$ which corresponds to the $c = \beta$ solutions. The solutions for $q_0 \leq q_0^*$ are cut off at $q_0 = q_0^c$ where the slope at $x = L$ is equal to the threshold $-\mu_b$ (big dot). The important point is that this curve $M(q_0)$ is a decreasing function, which make these domes unstable. In the inset, the inverse of the velocity $1/c$ is plotted against a typical size $M^{1/2}$ of the dome. It is strictly constant for $M \leq M(q_0^*)$ and then almost straight up to the cut-off value of M.

dome corresponds to the minimal disturbance needed to create a dune. We will see in the conclusion that the dome solutions may also play an important role when extending the present model to three dimensional situations.

4.3 Dunes

Dunes are stabilised by the presence of the slip face and the recirculation bubble, contrarily to domes. Because no grains can escape from the slip face, the net out flux and thus q_0 are null. Note that this is particular to two-dimensional situations that we are focused on: three dimensional barchan dunes loose sand from their horns. In our approach, the effect of the recirculation bubble on the wind is simply to modify the total length of the dune D which becomes the dune length L plus the bubble length R: $D = L + R$, as shown in Figure 2. The importance of the recirculation bubble becomes very clear: because it makes the apparent length of the dune larger, it increases the erosion at the top of the dune, due to the curvature effect.

As for the upwind foot of the dune, the boundary condition at the brink is determined dynamically. Consider first the expression (6) of the saturated flux. In the way the recirculation bubble is modelled, the convolution term should be computed on the profile h composed by the soil, plus the dune surface, plus the separation streamline (Fig. 2). The brink boundary condition is thus determined by the assumption that the transition – for the wind and thus the saturation flux – between the dune and the separation streamline is smooth. Therefore, the curvature at $x = L$ must also be continuous, as observed when integrating numerically equations (6, 15, 16). Assuming that the boundary layer reattaches on the flat soil downwind the dune equation (8), it gives:

$$h''(L) = h_b''(L) = -\frac{6B/R + 4p}{R} \cdot \tag{24}$$

We have checked that other choices for the parametrizing of the separation streamline do not change the qualitative conclusions presented below. In a general way, the recirculation bubble conditions can be expressed as $R/B = f_1(p)$ and $h''(L)B = f_2(p)$, where the functions f_1 and f_2 encode the particular choice of the streamline separation profile h_b.

Using the boundary conditions together with the explicit expression of the dune profile (20), one obtains three relations linking together the four parameters c, L, R and B. Instead of plotting, say, the three first with respect to the last one, we rather chose to express, as we did for the domes in the previous section, all of them as functions of the total mass M of the dune:

$$M = \int_0^L \mathrm{d}x\, h(x) + \frac{B^2}{2\tan\varphi} \cdot \tag{25}$$

We then get a continuous set of dune solutions, from very large values of the mass, down to some cut-off value M_c below which the turbulent boundary layer does not separate from the dune any more. With the criterion previously defined, this cut-off corresponds to the dune for which the maximum slope – at the inflexion point – is equal to the critical slope $-\mu_b$ and is achieved at the brink. In Table 1, mass, velocity and height of the smallest dune solution are compared to that of the largest dome – for both, the steepest slope is equal to $-\mu_b$. Consistently, these data are pretty close to each other.

Table 1. Mass, velocity and height of the smallest dune solution compared to that of the largest dome – for both, the steepest slope is equal to $-\mu_b$. Consistently, these data are pretty close to each other. These numerical values have been computed with $\alpha = 1$, $\beta = 4$ and $\mu_b = 0.25$.

	M	c	H
Smallest dune	3.55	3.19	0.71
Largest dome	6.55	2.78	0.78

Let us fix a value of the mass of sand M available to construct a dune. As for the domes, even for the simple choice of the recirculation bubble profile (8), a numerical resolution is required at this point to get the corresponding values of the parameters c, L, R and B. Three examples of such solutions are plotted in Figure 10. As evidenced in Figure 11, when rescaled by a typical dimension of the dune – here the square root of the mass –, the different profiles do not collapse on a single curve. In particular the slope at the brink $p = h'(L)$ varies with respect to M, and even changes its sign for this choice of the parameters α, β and μ_b. We get $p < 0$ for the smallest dune,

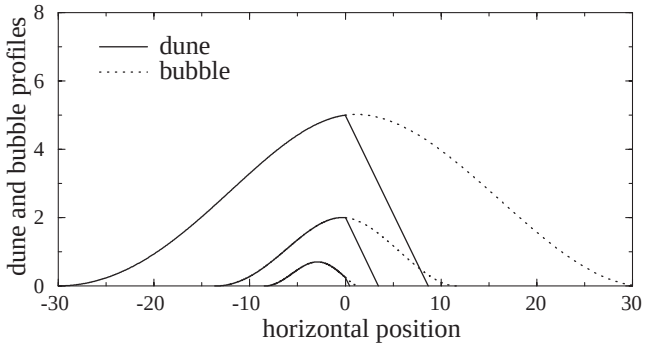

Fig. 10. Dunes of different masses and corresponding recirculation bubbles. From small to large, the masses are $M = 3.55$, 16.6 and 88.7. The other parameters are $\alpha = 1$, $\beta = 4$ and $\mu_b = 0.25$. For clarity, all these profiles have been shifted in order to get all brink positions at $x = 0$.

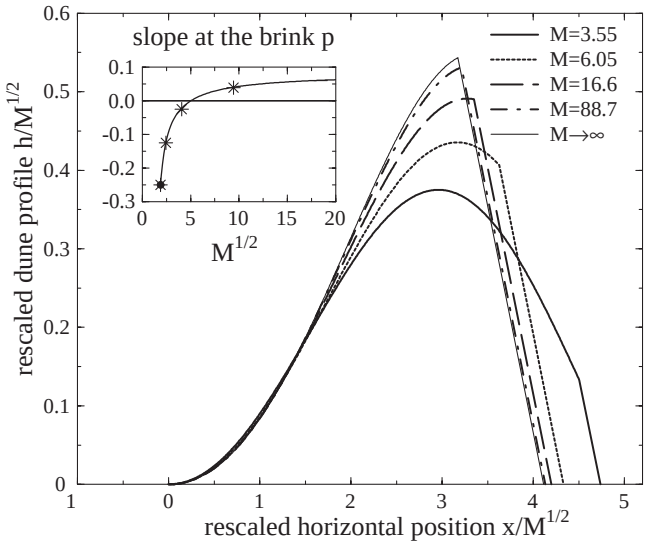

Fig. 11. Rescaled profiles of dunes of different sizes. The data have been computed with $\alpha = 1$, $\beta = 4$ and $\mu_b = 0.25$. Lengths have been rescaled by the square roots of the masses of the dunes. These profiles are not scale invariant: as shown in the inset, the slope p just before the brink is negative for small dunes and positive for large ones, such that depending on the dune size, the crest does or does not coincide with the brink. The four stars represent the four dune profiles. The smallest one ($M = 3.55$) coincides with the critical size (big dot).

while $p > 0$ for the largest one. The inset of Figure 11 as well as the curves of Figures 12 and 13 show the dune and bubble features (lengths, slope, aspect ratios and velocity) as a function of the mass of the dune M. The results are remarkably simple: as actual dunes, the lengths L, R, H and B are almost straight lines as a function of the dune size $M^{1/2}$. Similarly, $1/c \sim aM^{1/2} + b$ with a very good precision. At last, it must be noted that the dune and bubble aspect ratios are not constant: large dunes are more compact with a proportionally larger bubble than small ones.

Let us complete these results by a parametric study of the minimal dune heights H_c and B_c and the dune slope

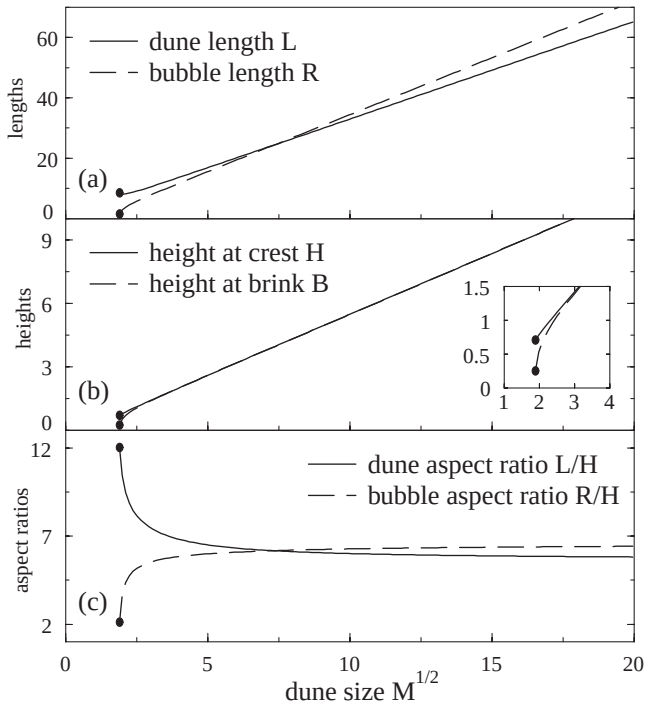

Fig. 12. Scaling of the lengths L, R (a) and H, B (b) with the dune size $M^{1/2}$. As a first approximation, these plots are almost straight lines. They are cut off at a critical mass (big dot) corresponding to a dune for which the steepest slope is equal to the critical value $-\mu_b$ at the brink. The inset on graph (b) is a zoom around this cut-off scale. Graph (c) shows that the dune and bubble aspect ratios are not constant: large dunes are more compact with a proportionally larger bubble than small ones. The data have been computed with $\alpha = 1$, $\beta = 4$ and $\mu_b = 0.25$.

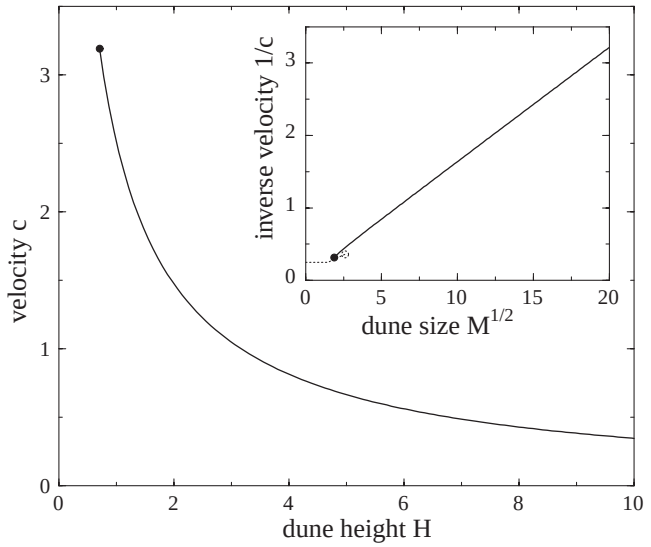

Fig. 13. Propagation velocity c of the dune as a function of its height H. As shown in the inset, with a very good precision, $1/c \sim aM^{1/2} + b$ down to some cut-off value. The dashed line and dashed circle correspond to the dome solution (see Fig. 9). These data have been computed with $\alpha = 1$, $\beta = 4$ and $\mu_b = 0.25$.

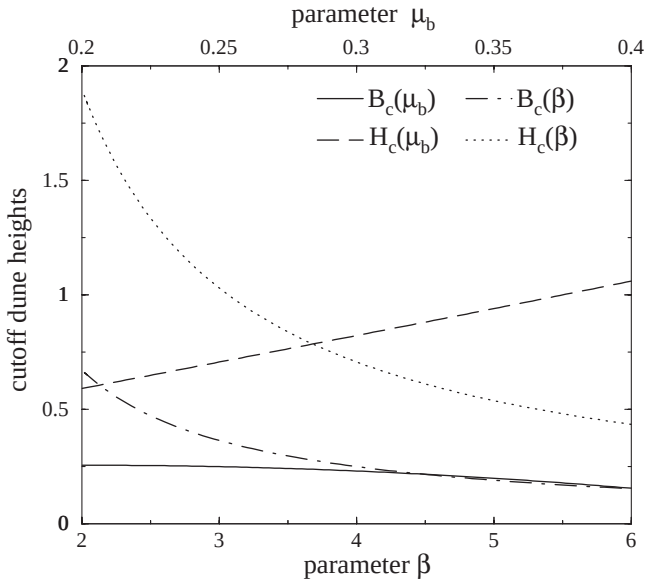

Fig. 14. Variations of the minimal dune heights H_c and B_c with the parameters β and μ_b. To plot theses curves, we took $\alpha = 1$.

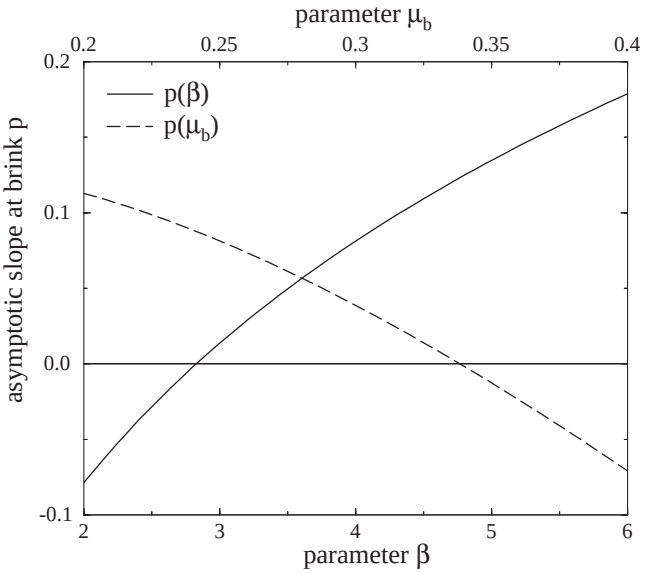

Fig. 15. Variation of the asymptotic ($M \to \infty$) slope at the brink p with the parameters β and μ_b. To plot theses curves, we took $\alpha = 1$. Besides, the solid line has been obtained with $\mu_b = 0.25$, and the dashed one with $\beta = 4$. Interestingly, p remains negative for small β or large μ_b.

at the brink of asymptotically large dunes ($M \to \infty$). The parameter α is kept to unity, but β has been varied between 2 and 6, and μ_b from 0.2 to 0.4. Figure 14 shows that the corresponding variations of H_c and B_c are not very strong. Similarly, the aspect ratio of very large dunes is always of the same order of magnitude. The most interesting fact is perhaps that for small values of β, or for large values of μ_b, the slope at the brink of very large dunes could have remained negative – see Figure 15. In that case, the brink and the crest are always distinct, even for asymptotically large dunes.

One can understand intuitively the variations of H_c, B_c and p with β and μ_b. Increasing β gives more strength to the destabilizing process, which lets small dunes appear at lower critical scale (smaller H_c and B_c) and makes large dunes more bumpy (larger p). If μ_b gets larger, the minimal allowed dune can be smaller (H_c decreases with μ_b), but with a corresponding larger brink height B_c. On large dunes, steep bubbles impose a negative slope at the brink.

5 Conclusion

We have shown in this paper how, inspired from the work of Sauermann *et al.*, one can build a simpler two dimensional model for the formation and the propagation of dunes. This modelling is based on two main variables: the dune profile h and the volumic sand flux q and includes three effects: (i) the mass conservation, (ii) the space lag over a length l_{sat} for the sand flux to become saturated at some value q_{sat}, and (iii) the feedback of the profile on the saturated flux. In this third phenomenological equation, erosion and deposition processes are the result of the competition between two antagonist mechanisms: a stabilizing non local curvature term (α) and a destabilizing slope one (β) which breaks the upwind-downwind symmetry.

Two kinds of solutions have been found: so-called 'domes' which do not show any avalanche slip face, and 'dunes' for which a downwind recirculation bubble has been introduced. We were able to predict an analytical form for their propagative profiles, but whose coefficients have to be computed numerically.

The results of the model resemble very much field observations. We found for example that, due to this length scale l_{sat}, the dune profiles are not scale invariant: small dunes are flatter than large ones. Another point is that the inverse of the propagative velocity c is, to a very good precision, almost linear with the size of the dune. This is consistent with Bagnold's argument that $c \simeq q_{sat}/H$ for a dune of height H. In fact, this relation overestimates the velocity of small dunes for which the sand flux may not be already saturated at the crest and also because, compared to large dunes, the value of q_{sat} is reduced due to a smaller curvature.

An important point discussed all through the paper was the issue of the boundary conditions. In particular, an important physical input was the 'recirculation bubble' behind the dune. This bubble makes the dune effectively look larger to the wind, and, due to the non local term in the relation between the saturated flux and the dune profile, has a stabilizing role. In fact, very little is known and well established about this recirculation bubble, but most of the dune features (position of the slip face, cut-off size, etc.) precisely depend on fine interactions and feedbacks between the dune and the bubble. More studies on this point are needed.

Another central result of the paper is the existence of a cut-off scale, below which no dune solution exits. It corresponds to the dune for which the steepest slope is equal to the critical value $-\mu_b$ needed to make the bubble appear. Not surprisingly, this scale is of order of l_{sat}. This result then rises the question of dune initiation and formation. The two scenari usually proposed by geophysicists for the formation of dunes are the following: first possibility, a small bump (of the size of ripples) grows continuously and forms a dune; second one, the sand accumulates on a solid obstacle like a rock or a bush and, when the size of the accumulation becomes larger than the obstacle, a dune forms and starts propagating downwind. However, observations show that ripples are stable and no structures between dunes and ripples can be seen. Similarly, rocks and bushes create lee dunes of the size of the obstacle but which remain anchored to the obstacle. An alternative explanation can be proposed, following the results of the stability analysis of the equations of the model, as well as that of the dome solutions. We found that large wavelengths perturbations get amplified, and that the dome profiles, selected by their incident flux q_0, are unstable to changes of that flux. Then, a possibility is that first domes form with a small height but directly with large length and width, and second that these domes, by this flux instability, progressively become more and more compact, and eventually reach the point where their slope is steep enough to generate a bubble and create an avalanche slip face to become an actual dune.

Several extensions to the present work can be thought of. First, we would like to go beyond the calculation of purely propagative solutions, and study the full dynamics of a given dune profile. In particular, as just said, an important point is the evolution of the dome solutions when submitted to incident sand flux variations. A second point is to go from a 2d description – transverse dunes – to real three dimensional situations. The idea is to 'cut a barchan into longitudinal 2d slices'. As a matter of fact, a barchan slice close to the center of the dune looks like our dune solution, while a slice made at the edges where the horns are present rather have a dome shape. Suppose these slices are completely decoupled. Because the small ones go faster than the large ones, an initial conical sandpile will soon get a crescentic shape. However, when equilibrium is reached, all the slices should move at the same velocity. There should thus be a coupling between them, namely a lateral sand flux from the centre towards the horns. When the flux is saturated at the crest the velocity at the crest is $c = (q_{sat} - q_0)/H$. This suggests than an equilibrium can indeed be achieved if q_0 increases in the small slices. Eventually the 3d dune slip face will be the sum of the contributions of all 2d slices whose brinks depend on their heights. Note that this scenario is consistent with the field observation that barchan horns are more elongated at strong winds which make the lateral sand flux less important, and consequently slices less coupled.

Finally, quantitative comparisons between experimental dune profiles and our theoretical predictions will be performed. This idea is to use barchan longitudinal slices as that shown in Figure 7, but also sand structures under water, such as those obtained by Betat *et al.* [10] or Andersen *et al.* [11] for which, in principle, this model should be also valid.

We are grateful to G. Sauermann and K. Kroy for precise explanations of all the details of their modelling. The measurements of the dune profiles (Fig. 7) were performed by B. Andreotti, S. Douady, P. Hersen and L. Quartier. P.C. wish to thank C. Krülle and B. Murray for useful discussions. This work benefited from the 'Action Concertée Inicitative Jeunes Chercheurs' of the French Ministry of Research.

Appendix: the low flux dome solution

How can we construct a dome solution for $q_0 < q_0^*$? Suppose the values of the velocity c and the length D are given, from equation (20) we can compute h and its derivatives as well as q_{sat}. Because q_0 is smaller than q_0^*, q_{sat} will reach zero at some position $x = L < D$. Negative values of q_{sat} are not permitted, and we therefore set it to zero for $x \geq L$. Then, equation (16) is very easy to integrate and gives and exponential branch for the flux $q(x)$, which, using the linear relation (18) between q and h leads to:

$$h_r(x) = \frac{1}{c}\left[(cH_r + q_0)\mathrm{e}^{-(x-L)} - q_0\right]. \qquad \text{(A.1)}$$

The subscript r is used to avoid any confusion with $h(x)$ given by equation (20), but both are part of the same smooth dome solution. Now, if one compute what would be the saturated flux q_{sat}^r calculated from the profile h_r with the relation (17), one sees that it is negative as it should be close to $x = L$ (remember that q_{sat} is set to zero), but crosses zero at some other position $x = L + R < D$. From that point and for larger x we thus need to come back to the original profile h. Then, a natural way to end up the dome profile is to use

$$h_y(x) = h(D - x), \qquad \text{(A.2)}$$

which is consistent if $q_{sat}(-Y) = 0$, with $L + R + Y = D$. This choice ensures that both $h(D)$ and $h'(D)$ vanish as required. These three regions of the dome solution are illustrated in Figure 16.

Let us now be more explicit about the continuity conditions at the two matching points. At $x = L$, by construction of the relation (A.1), the dome profile, the sand flux, and the saturated flux are continuous. Because equation (16) holds everywhere, it implies that $\partial_x q$, and therefore the slope h' are also continuous. By contrast, the curvatures $h''(L)$ and $h_r''(L)$ are different, and therefore $q_{sat}^r(L) \neq q_{sat}(L) = 0$. The position $x = L + R$ is defined by $q_{sat}^y(L + R) = q_{sat}(-Y) = 0$. At this point of course we do not want any step in the dome profile, such that $H_y \equiv h_y(L + R)$ and $h_r(L + R)$ must be equal. Again, because of equation (16) and the fact that q_{sat} has been built to be continuous at $x = L + R$, the continuity of the

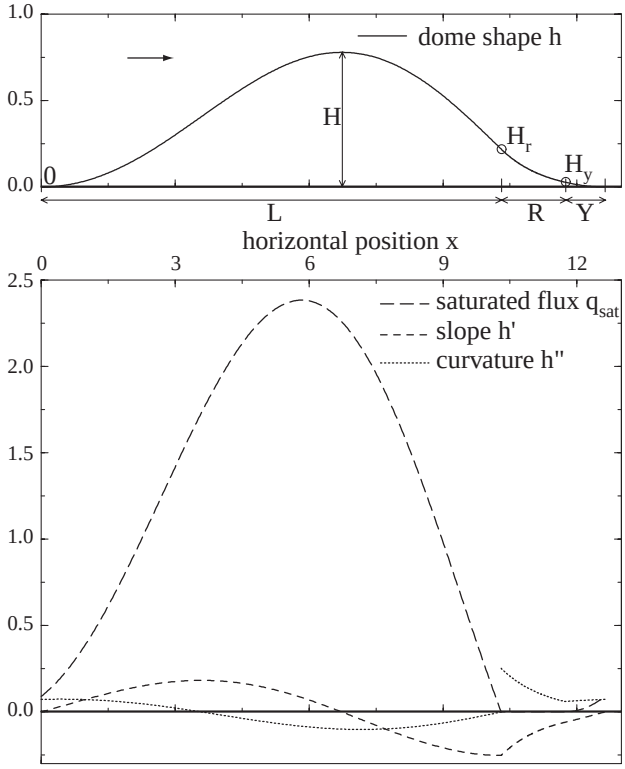

Fig. 16. Top: Profile of a dome. Bottom: Slope, curvature and saturated flux in the same conditions. H is the dome height. As $q_0 < q_0^*$, its length D must be cut into three regions of size L, R and Y. The saturated flux q_{sat} is strictly zero between $x = L$ and $x = L+R$ and the profile is a branch of exponential which matches with the two parts of the full solution. H_r and H_y are the heights at the two sides of this central region. At $x = L$ the curvature h'' shows a discontinuity, but all quantities are continuous at $x = L + R$. With the sand supply chosen ($q_0 = 0.09$), the dome steepest slope just reaches its minimum permitted value $-\mu_b$ at $x = L$.

profile makes the slope continuous too. However this position is also the point where the pseudo saturated flux q^r_{sat} crosses zero, such that the curvature of the dome profile is also continuous. All these continuity conditions can be shown in Figure 16.

To sum up, we have in practice four coefficients to determine: c, L, R and Y ($D = L + R + Y$) with the four non-linear following equations: $q_{sat}(L) = 0$, $q_{sat}(-Y) = 0$, $h_r(L+R) = h(-Y)$ and $q^r_{sat}(L+R) = 0$. These equations can then be solved numerically. One can find such a solution for any $q_0 < q_0^*$ but it is valid only if its steepest slope is larger than $-\mu_b$. This fixes a lower bound q_0^c under which there is no consistent solution. With $\alpha = 1$, $\beta = 4$ and $\mu_b = 0.25$, $q_0^c \simeq 0.09$, flux for which the dome is shown in Figure 16.

References

1. R.A. Bagnold, *The physics of blown sand and desert dunes* (Chapman and Hall, London, 1941)
2. G. Sauermann, Ph.D. thesis, Stuttgart University, edited by Logos Verlag (Berlin, 2001)
3. G. Sauermann, K. Kroy, H.J. Herrmann, Phys. Rev. E **64**, 031305 (2001)
4. K. Kroy, G. Sauermann, H.J. Herrmann, Phys. Rev. Lett. **88**, 054301 (2002)
5. K. Kroy, G. Sauermann, H.J. Herrmann, *Minimal model for aeolian sand dunes*, `cond-mat/0203040`
6. R.S. Anderson, P.K. Haff, Science **241**, 820 (1988)
7. B. Peer, V. Hakim, private communication
8. P.S. Jackson, J.C.R. Hunt, Quart. J. R. Met. Soc. **101**, 929 (1975)
9. W.S. Weng, J.C.R. Hunt, D.J. Carruthers, A. Warren, G.F.S. Wiggs, I. Livingstone, I. Castro, Acta Mechanica **2**, 1 (1991)
10. A. Betat, C.A. Krülle, V. Frette, I. Rehberg, *Long-time behaviour of sand ripples induced by water shear flow*, submitted to Eur. Phys. J. E
11. K. Andersen, P. Gondret, M. Rabaud, T. Loiseleux, private communication
12. N.-O. Jensen, O. Zeman, in *International workshop on the physics of blown sand*, edited by O.E. Barndorff-Nielsen, K. Moller, K.R. Rasmussen, B.B. Willets (University of Aarhus, 1985), pp. 351–368